DEPARTMENT OF DEFENCE
DEFENCE SCIENCE & TECHNOLOGY ORGANISATION
DSTO

On the Choice of the Coordinate System and Tracking Filter for the Track-while-scan Mode of an Airborne Pulse Doppler Radar

Steven Zollo and Branko Ristic

DSTO-TR-0926

On the Choice of the Coordinate System and Tracking Filter for the Track-while-scan Mode of an Airborne Pulse Doppler Radar

Steven Zollo and Branko Ristic

Surveillance Systems Division
Electronics and Surveillance Research Laboratory

DSTO–TR–0926

ABSTRACT

A comparison between tracking in *spherical coordinates* using coupled range and angle filters and tracking with debiased consistent converted measurements in 3D *Cartesian coordinates* is presented. The sensor is an airborne pulse Doppler radar (APDR) with typical measurements being range, range-rate, azimuth and elevation. The report investigates the tracking accuracy (position, range-rate and vertical/horizontal heading) achievable in the Medium and High PRF mode of an APDR, for both non-manoeuvring and manoeuvring targets. The manoeuvre handling logic is based on the interactive multiple model (IMM) approach.

Published by

DSTO Electronics and Surveillance Research Laboratory
PO Box 1500
Salisbury, South Australia, Australia 5108

Telephone: (08) 8259 5555
Facsimile: (08) 8259 6567

AR No. AR-011-191
December, 1999

APPROVED FOR PUBLIC RELEASE

On the Choice of the Coordinate System and Tracking Filter for the Track-while-scan Mode of an Airborne Pulse Doppler Radar

EXECUTIVE SUMMARY

This report is part of a study into the performance of the Track-While-Scan (TWS) mode of an airborne pulse Doppler radar, and as such represents a contribution to the Australian Hornet Upgrade (HUG) programme.

The subject of the report is the choice of the coordinate system and the tracking filter for the TWS algorithm. The evaluation of various filter options is based on the tracking accuracy (quality) which is an important performance measure from the standpoint of tactical weapons launch. Poor track quality reduces the probability of a kill at a given range. In the report we consider two common coordinate systems for tracking: spherical and Cartesian. After introducing two types of tracking filters (one for spherical and the other for Cartesian coordinates) we incorporate the interactive multiple model (IMM) logic into both of them in order to be able to track the manoeuvring targets.

Extensive computer simulations have been performed to test the tracking quality in terms of the positional, vertical/horizontal heading and the range-rate errors. The results can be summarised as follows:

- The Cartesian tracker is more accurate during the non-manoeuvring segments of the target trajectory;
- The spherical tracker is more accurate during the manoeuvring segments;
- Range-rate measurements increase the tracking accuracy only in the high pulse repetition frequency mode;
- The Cartesian tracking filter is slightly more computationally intensive than the spherical filter.

Overall the spherical coordinate system seems to be a reasonable choice for a tracking filter in an airborne pulse Doppler radar, being fairly robust to manoeuvres and simple to implement. The design of a tracking filter in Cartesian coordinates requires more attention to the choice of the dynamic models in IMM logic; its main advantage is better accuracy for non-manoeuvring segments of a target trajectory.

Authors

Steven Zollo
Surveillance Systems Division

Steven Zollo completed his BE(elect) at the University of Adelaide in 1999. He joined DSTO in February 1999 as a professional officer, providing software support in the areas of tracking and sensor fusion. His main research interest is currently airborne tracking systems.

Branko Ristic
Surveillance Systems Division

Branko Ristic completed a BEng and MSc in Elec. Eng. at the University of Novi Sad and Belgrade University (Yugoslavia) in 1984 and 1991 respectively. He received a PhD from the Signal Processing Research Centre (QUT, Brisbane) in 1995. Between 1984 to 1989 he was a research engineer in the Vinca Institute in Belgrade. In February 1989 he arrived in Australia and since then he has been a senior research assistant at The University of Queensland (1989-1991) and QUT (1991-1993), senior DSP engineer in GEC Marconi Systems (1995) and Research Fellow at QUT (1996). In May 1996 he joined DSTO where he was initially working on enhancements to the Jindalee tracker. He is currently a Senior Research Scientist responsible for tracking and multi-sensor integration on airborne platforms. His main research interests include tracking and estimation theory.

Contents

Figures

Tables

Glossary

3D Three-dimensional

APDR Airborne pulse Doppler radar

HPRF High pulse repetition frequency

IMM Interactive multiple model

KF Kalman filter

EKF Extended Kalman filter

MPRF Medium pulse repetition frequency

RMS Root mean square

TWS Track-While-Scan

AMRAAM Advanced Medium Range Air to Air Missile

NED North-East-Down

1 Introduction

Track accuracy is one of the most important performance measures of a tracking system from the standpoint of tactical weapons launch in an air-to-air engagement. Excessive track errors (in target position or heading for example) reduce the "probability of kill" by semi-autonomous weapons (such as AMRAAM). This is due to the requirement for a regular update of target position/velocity through the entire flight of the missile up to the point at which the seeker head goes active. In order to support the missile and at the same time maintain the pilot's situational awareness, the track-while-scan (TWS) mode of the airborne pulse Doppler radar (APDR) is used. If there is a demand to keep the "probability of kill" at a given level, in the presence of excessive track errors the limit of the engagement launch of the missile has to be reduced.

Track accuracy in general depends on the quality of measurements (their accuracy and update rate) and the design of the tracking filter. A radar signal processor unit is responsible for the quality of measurements, while the designer of a tracking system selects the tracking coordinate system, filter state variables and the tracking filter algorithm. In this report we assume that the sensor is an airborne pulse Doppler radar with measurements which include target range ρ_m, range-rate $\dot{\rho_m}$, azimuth θ_m and elevation ϵ_m.

As for the choice of the tracking filter, two common coordinate systems have been used: spherical and Cartesian [2, Sec. 3.7]. The advantage of Cartesian coordinates is that the state equation is linear (linear target dynamic model) but its drawback is that the corresponding measurement equation is non-linear. The non-linearity of measurements can be handled either by the use of the extended Kalman filter (EKF) or by converting the measurements to Cartesian coordinates prior to filtering. This second approach, if carried out properly (conversion is debiased and consistent), is exact and therefore preferred [9], [12], [13]. Disadvantages of Cartesian coordinates are: (1) measurements are coupled and as a consequence, the calculations, such as matrix inversions, are computationally intensive; (2) range measurements must be available (which in some situations, such as in the presence of electronic countermeasures, may not be the case) [3, p.59].

If spherical coordinates are selected, the state equation of a constant velocity target is non-linear while the measurement equation is linear. The consequence of a non-linear state equation is that even a constant velocity target produces accelerations in angle (so-called pseudo-accelerations), and therefore higher-order derivatives are required in the system model (see for more details [6, Sec. 1.5]). To alleviate this problem, a suboptimal tracking filter in spherical coordinates has been developed [3, Sec. 3.5]. It consists of a separate range/range-rate filter and three angle filters. Being simple and reliable, the tracking filter in spherical coordinates has been utilised in a number of operational tracking systems [6].

It is generally accepted that tracking in Cartesian coordinates is more accurate but more computationally intensive [7]. For distant targets, tracking in spherical coordinates may be adequate, since the pseudo-acceleration is small [6]. Following the theory presented in [9] and [12], this paper develops a tracking filter based on 3D (range, azimuth, elevation) debiased consistent converted measurements and with incorporated range-rate measurements. The tracking accuracy (position, horizontal/vertical heading, range-rate) of this filter is then compared to the accuracy of the tracking filter in spherical coordinates (described in [3, Sec. 3.5]) as well as to the Cartesian filter which does not use range-rate

measurements. To enable tracking of the manoeuvring targets, the interactive multiple model (IMM) logic [1, p.461] has been incorporated into both spherical and Cartesian tracking filters. The report is organised as follows. Section 2 presents the tracking filters in spherical and Cartesian coordinates, section 3 details the IMM extensions of the filters. Section 4 describes the comparison methodology and simulation results. Section 5 is devoted to conclusions.

2 Tracking Filters

The dynamic motion equation for both spherical and Cartesian coordinates is given by:

$$\mathbf{s}_{k+1} = \mathbf{F}_k \mathbf{s}_k + \mathbf{v}_k + \mathbf{g}_k \tag{1}$$

where $\mathbf{s}$ is the state vector, $\mathbf{F}$ is the transition matrix, $\mathbf{v}$ is process noise and $\mathbf{g}$ is the own-ship motion compensation vector. Index k is a discrete time index.

2.1 Spherical Coordinates

For tracking in spherical coordinates a processing scheme described in [3, Sec. 3.5] has been implemented. This scheme consists of four Kalman filters (KFs) running in parallel: one range/range-rate KF and three direction cosine KFs (for north, east and down directions).

The various components of the state equation 1 for the **range/range-rate filter** are as follows. The state vector is $\mathbf{s}_R = [R\ \dot{R}\ \ddot{R}]'$ where R is the range. The transition matrix is:

$$\mathbf{F}_R = \begin{bmatrix} 1 + \frac{\omega_p^2 T^2}{2} & T & \frac{T^2}{2} \\ \omega_p^2 T & 1 + \frac{\omega_p^2 T^2}{2} & T(1 - \frac{T}{2\tau_R}) \\ 0 & 0 & e^{-T/\tau_R} \end{bmatrix}$$

where τ_R is the manoeuvre time constant; T is the sampling interval; ω_p is the angular rate perpendicular to the line-of-sight vector to the target (its estimate comes from the direction cosine filters). The own-ship compensation vector expresses the contribution due to own-ship acceleration a_{O} in the radial direction, i.e.

$$\mathbf{g}_R = [-\frac{T^2}{2} a_{\mathrm{OR}} \quad -T a_{\mathrm{OR}} \quad 0]'$$

The covariance matrix of process noise $\mathbf{v}$ in (1) is given by eqn. (2.17) of [3].

The components of the state equation 1 for a **direction cosine filter** (one of the three) are as follows. The state vector is $\mathbf{s}_{\lambda_{\mathrm{N,E,D}}} = [\lambda \quad v \quad a_T]'_{\mathrm{N,E,D}}$, where $\lambda_{\mathrm{N,E,D}}$ is a direction

cosine defined as:

$$\begin{aligned}
\lambda_N &= \cos\epsilon\,\cos\theta = \frac{R_N}{R} \qquad \text{(north direction)} \\
\lambda_E &= \cos\epsilon\,\sin\theta = \frac{R_E}{R} \qquad \text{(east direction)} \\
\lambda_D &= -\sin\epsilon = \frac{R_D}{R} \qquad \text{(down direction)}
\end{aligned}$$

with R_N (R_E, R_D) being the component of target position in north (east, down) direction. The second and third states in the state vector of the north direction cosine filter are defined as: $v_N = \dot{R}_N$, and $a_{\text{TN}} = \ddot{R}_N + a_{\text{ON}}$ where a_{ON} is own-ship acceleration in the north direction. The transition matrix for (all three) direction cosine filters is given by:

$$\mathbf{F}_\lambda = \begin{bmatrix} 1 - \frac{\dot{R}T}{R}(1 - \frac{\dot{R}T}{2R}) & \frac{T}{R}(1 - \frac{\dot{R}T}{2R}) & \frac{T^2}{2R} \\ 0 & 1 & T(1 - \frac{T}{2\tau_m}) \\ 0 & 0 & e^{-T/\tau_m} \end{bmatrix} \tag{2}$$

where τ_m is the manoeuvre time constant. The range R and range-rate $\dot{R}$ in (2) are obtained from the range/range-rate filter. The own-ship vector for a north direction cosine state equation is given by:

$$\mathbf{g}_{\lambda_N} = \begin{bmatrix} -\frac{a_{\text{ON}}T^2}{2R} & -a_{\text{ON}}T & 0 \end{bmatrix}'$$

The covariance of process noise $\mathbf{v}$ in direction-cosine state equations is given by eqn. (2.17) of [3] with the exception that the elements of the first (direction cosine) state are modified as follows: $q'_{11} = q_{11}/R^2$, $q'_{12} = q_{12}/R$ and $q'_{13} = q_{13}/R$.

In summary, the four filters for tracking in spherical coordinates are coupled in the following sense: (i) the estimated range and range-rate from the range/range-rate KF are used in prediction of the direction cosine KFs; (ii) the estimated angular rate ω_p calculated from the three direction cosine KFs is used for prediction in the range/range-rate KF. An approximate calculation of ω_p is as follows [3, Sec. 3.5]:

$$\omega_p^2 = \frac{(v_{\text{N}}\lambda_{\text{E}} - v_{\text{E}}\lambda_{\text{N}})^2 + v_{\text{D}}^2}{R^2}$$

Note that the described processing scheme for tracking in spherical coordinates (referred to as *Spherical* further in the text) is based on linear state equations. As such it has been derived from a number of reasonable approximations (for airborne surveillance) and hence it has found application in a number of operational systems [6, Sec. 1.5].

2.2 Cartesian Coordinates

For tracking in Cartesian coordinates, debiased consistent converted measurements of range, azimuth and elevation were used. The range-rate measurements are also incorporated via the second order KF [8]. The x, y and z direction are used (by convention) to correspond to east, north and down direction. The following steps were used in the development of the tracking filter in Cartesian coordinates.

(I) Conversion of radar measurements ρ_m, θ_m and ϵ_m:

$$\begin{aligned} x'_m &= \rho_m \cdot \cos\theta_m \cdot \cos\epsilon_m \\ y'_m &= \rho_m \cdot \sin\theta_m \cdot \cos\epsilon_m \\ z'_m &= -\rho_m \cdot \sin\epsilon_m \end{aligned} \tag{3}$$

(II) Debiasing of measurements. Assuming that measurements of range, azimuth and elevation are zero mean Gaussian with diagonal covariance matrix with elements along the diagonal being σ_ρ^2, σ_θ^2 and σ_ϵ^2, the debiasing is done as follows [1] [12]:

$$\begin{aligned} x_m &= x'_m[1 - (e^{-\sigma_\theta^2}\, e^{-\sigma_\epsilon^2} - e^{-\sigma_\theta^2/2}\, e^{-\sigma_\epsilon^2/2})] \\ y_m &= y'_m[1 - (e^{-\sigma_\theta^2}\, e^{-\sigma_\epsilon^2} - e^{-\sigma_\theta^2/2}\, e^{-\sigma_\epsilon^2/2})] \\ z_m &= z'_m[1 - (e^{-\sigma_\epsilon^2} - e^{-\sigma_\epsilon^2/2})] \end{aligned} \tag{4}$$

(III) Covariance matrix of converted measurements x_m, y_m and z_m:

$$\mathbf{R}_a = \begin{bmatrix} R_a^{xx} & R_a^{xy} & R_a^{xz} \\ R_a^{xy} & R_a^{yy} & R_a^{yz} \\ R_a^{xz} & R_a^{yz} & R_a^{zz} \end{bmatrix} \tag{5}$$

where the expressions for elements of $\mathbf{R}_a$ are given in [12].

(IVa) State equation (constant velocity motion). The state vector in eqn. (1) is given by $\mathbf{s}_k = [x_k\ \dot{x}_k\ y_k\ \dot{y}_k\ z_k\ \dot{z}_k]'$. The transition matrix is

$$\mathbf{F} = \begin{bmatrix} 1 & T & 0 & 0 & 0 & 0 \\ 0 & 1 & 0 & 0 & 0 & 0 \\ 0 & 0 & 1 & T & 0 & 0 \\ 0 & 0 & 0 & 1 & 0 & 0 \\ 0 & 0 & 0 & 0 & 1 & T \\ 0 & 0 & 0 & 0 & 0 & 1 \end{bmatrix}$$

and the covariance matrix of $\mathbf{v}_k$ is taken from the Singer model:

$$\mathbf{Q} = \frac{2\sigma_m^2}{\tau_m} \begin{bmatrix} q_{11} & q_{12} & 0 & 0 & 0 & 0 \\ q_{12} & q_{22} & 0 & 0 & 0 & 0 \\ 0 & 0 & q_{11} & q_{12} & 0 & 0 \\ 0 & 0 & q_{12} & q_{22} & 0 & 0 \\ 0 & 0 & 0 & 0 & q_{11} & q_{12} \\ 0 & 0 & 0 & 0 & q_{12} & q_{22} \end{bmatrix}$$

where σ_m is the manoeuvre standard deviation, τ_m is the manoeuvre time constant and q_{11}, q_{12} and q_{22} are given by eqn. (2.17) in [3]. The ownship compensation vector in (1) in this case is:

$$\mathbf{g} = -[a_{\mathrm{Ox}}T^2/2\ \ a_{\mathrm{Ox}}T\ \ a_{\mathrm{Oy}}T^2/2\ \ a_{\mathrm{Oy}}T\ \ a_{\mathrm{Oz}}T^2/2\ \ a_{\mathrm{Oz}}T]'$$

where a_{Ox} (resp. a_{Oy}, a_{Oz}) represents the own-ship acceleration in the x (resp. y,z) direction.

[1] Another scheme for unbiased spherical-to-Cartesian conversion of measurements has been reported in [13].

(IVb) State equation (constant acceleration motion). The state vector in eqn. (1) is given by $\mathbf{s}_k = [x_k\ \dot{x}_k\ \ddot{x}_k\ y_k\ \dot{y}_k\ \ddot{y}_k\ z_k\ \dot{z}_k\ \ddot{z}]'$. The transition matrix is

$$\mathbf{F} = \begin{bmatrix} \mathbf{f} & \mathbf{0} & \mathbf{0} \\ \mathbf{0} & \mathbf{f} & \mathbf{0} \\ \mathbf{0} & \mathbf{0} & \mathbf{f} \end{bmatrix}$$

where

$$\mathbf{f} = \begin{bmatrix} 1 & T & {\tau_m}^2(-1 + \frac{T}{\tau_m} + e^{-T/\tau_m}) \\ 0 & 1 & \tau_m(1 - e^{-T/\tau_m}) \\ 0 & 0 & e^{-T/\tau_m} \end{bmatrix}$$

and $\mathbf{0}$ is a 3x3 zero matrix. The covariance matrix of $\mathbf{v}_k$ is again from the Singer model:

$$\mathbf{Q} = \frac{2\sigma_m^2}{\tau_m} \begin{bmatrix} \mathbf{q} & \mathbf{0} & \mathbf{0} \\ \mathbf{0} & \mathbf{q} & \mathbf{0} \\ \mathbf{0} & \mathbf{0} & \mathbf{q} \end{bmatrix}$$

where

$$\mathbf{q} = \begin{bmatrix} q_{11} & q_{12} & q_{13} \\ q_{12} & q_{22} & q_{23} \\ q_{13} & q_{23} & q_{33} \end{bmatrix}$$

and q_{11}, q_{12}, q_{13}, q_{22}, q_{23} and q_{33} are given by eqn. (2.17) in [3]. The ownship compensation vector in (1) in this case is:

$$\mathbf{g} = -[a_{\mathrm{Ox}}T^2/2\ \ a_{\mathrm{Ox}}T\ \ 0\ \ a_{\mathrm{Oy}}T^2/2\ \ a_{\mathrm{Oy}}T\ \ 0\ \ a_{\mathrm{Oz}}T^2/2\ \ a_{\mathrm{Oz}}T\ \ 0]'$$

(V) Measurement equation. In addition to the three positional measurements, the range-rate, $\dot{\rho}_m$, is incorporated into the measurement equation. For this, the approach taken in [8, Sec. 4.6] is followed and is adapted to the case of the state vector defined here. The measurement vector is given by: $\mathbf{r}_k = [x_m\ y_m\ z_m\ \eta_m]'$ where η_m is calculated as $\eta_m = \rho_m\,\dot{\rho}_m$. The measurement equation is then:

$$\mathbf{r}_k = \mathbf{h}(\mathbf{s}_k) + \mathbf{w}_k$$

where

(a) for the constant velocity model, $\mathbf{h}(\mathbf{s}_k)$ is a column vector with 4 elements: $\mathbf{s}_k(1)$, $\mathbf{s}_k(3)$, $\mathbf{s}_k(5)$ and $\mathbf{s}_k(1)\mathbf{s}_k(2) + \mathbf{s}_k(3)\mathbf{s}_k(4) + \mathbf{s}_k(5)\mathbf{s}_k(6)$.

(b) for the constant acceleration model, $\mathbf{h}(\mathbf{s}_k)$ is a column vector with 4 elements: $\mathbf{s}_k(1)$, $\mathbf{s}_k(4)$, $\mathbf{s}_k(7)$ and $\mathbf{s}_k(1)\mathbf{s}_k(2) + \mathbf{s}_k(4)\mathbf{s}_k(5) + \mathbf{s}_k(7)\mathbf{s}_k(8)$.

The covariance matrix of $\mathbf{w}_k$ is given by:

$$\mathbf{R}_k = \begin{bmatrix} & \mathbf{R}_a & & \sigma_{x\eta} \\ & & & \sigma_{y\eta} \\ & & & \sigma_{z\eta} \\ \sigma_{x\eta} & \sigma_{y\eta} & \sigma_{z\eta} & \sigma_\eta^2 \end{bmatrix} \tag{6}$$

where the following relationships hold approximately $\sigma_\eta^2 = \sigma_\rho^2\sigma_{\dot{\rho}}^2 + \rho^2\sigma_{\dot{\rho}}^2 + \dot{\rho}^2\sigma_\rho^2$, $\sigma_{x\eta} = \dot{\rho}\,\sigma_\rho^2 \cos\theta\cos\epsilon$, $\sigma_{y\eta} = \dot{\rho}\,\sigma_\rho^2 \sin\theta\cos\epsilon$, $\sigma_{z\eta} = \dot{\rho}\,\sigma_\rho^2 \sin\epsilon$.

(VI) Second-order KF. The measurement equation is non-linear and a second-order KF [8] is employed for tracking. Its equations are:

$$\begin{aligned}
\hat{\mathbf{s}}_{k+1|k} &= \mathbf{F}\hat{\mathbf{s}}_{k|k} \\
\hat{\mathbf{P}}_{k+1|k} &= \mathbf{F}\hat{\mathbf{P}}_{k|k}\mathbf{F}' + \mathbf{Q} \\
\hat{\mathbf{r}}_{k+1|k} &= \mathbf{h}(\hat{\mathbf{s}}_{k+1|k}) + \mathbf{d}_{k+1|k} \\
\mathbf{B}_{k+1} &= \mathbf{H}(\hat{\mathbf{s}}_{k+1|k})\hat{\mathbf{P}}_{k+1|k}\mathbf{H}(\hat{\mathbf{s}}_{k+1|k})' + \mathbf{R}_{k+1} + \mathbf{A}_{k+1} \\
\mathbf{W}_{k+1} &= \hat{\mathbf{P}}_{k+1|k}\mathbf{H}(\hat{\mathbf{s}}_{k+1|k})'\mathbf{B}_{k+1}^{-1} \\
\hat{\mathbf{s}}_{k+1|k+1} &= \hat{\mathbf{s}}_{k+1|k} + \mathbf{W}_{k+1}(\mathbf{r}_{k+1} - \hat{\mathbf{r}}_{k+1|k}) \\
\hat{\mathbf{P}}_{k+1|k+1} &= \hat{\mathbf{P}}_{k+1|k} - \mathbf{W}_{k+1}\mathbf{B}_{k+1}\mathbf{W}_{k+1}'
\end{aligned}$$

where

(a) for the constant velocity model $\mathbf{d} = [0\ 0\ 0\ \hat{\mathbf{P}}(1,2) + \hat{\mathbf{P}}(3,4) + \hat{\mathbf{P}}(5,6)]'$, and $\mathbf{A}$ is a 4x4 matrix with all elements zero except for $\mathbf{A}(4,4)$ which can be worked out from [8, p.278] as:

$$\begin{aligned}
A(4,4) = {} & \hat{\mathbf{P}}(1,1)\hat{\mathbf{P}}(2,2) + \hat{\mathbf{P}}(3,3)\hat{\mathbf{P}}(4,4) + \hat{\mathbf{P}}(5,5)\hat{\mathbf{P}}(6,6) + \hat{\mathbf{P}}^2(1,2) + \hat{\mathbf{P}}^2(3,4) + \\
& \hat{\mathbf{P}}^2(5,6) + 2\hat{\mathbf{P}}(1,4)\hat{\mathbf{P}}(2,3) + 2\hat{\mathbf{P}}(1,6)\hat{\mathbf{P}}(2,5) + 2\hat{\mathbf{P}}(1,3)\hat{\mathbf{P}}(2,4) + \\
& 2\hat{\mathbf{P}}(1,5)\hat{\mathbf{P}}(2,6) + 2\hat{\mathbf{P}}(3,6)\hat{\mathbf{P}}(4,5) + 2\hat{\mathbf{P}}(3,5)\hat{\mathbf{P}}(4,6) \qquad (7)
\end{aligned}$$

Matrix $\mathbf{H}$ in this case is:

$$\mathbf{H}(\hat{\mathbf{s}}) = \begin{bmatrix} 1 & 0 & 0 & 0 & 0 & 0 \\ 0 & 0 & 1 & 0 & 0 & 0 \\ 0 & 0 & 0 & 0 & 1 & 0 \\ \hat{\mathbf{s}}(2) & \hat{\mathbf{s}}(1) & \hat{\mathbf{s}}(4) & \hat{\mathbf{s}}(3) & \hat{\mathbf{s}}(6) & \hat{\mathbf{s}}(5) \end{bmatrix}$$

(b) for the constant acceleration model $\mathbf{d} = [0\ 0\ 0\ \hat{\mathbf{P}}(1,2) + \hat{\mathbf{P}}(4,5) + \hat{\mathbf{P}}(7,8)]'$, and $\mathbf{A}$ is again a 4x4 matrix with all elements zero except for

$$\begin{aligned}
A(4,4) = {} & \hat{\mathbf{P}}(1,1)\hat{\mathbf{P}}(2,2) + \hat{\mathbf{P}}(4,4)\hat{\mathbf{P}}(5,5) + \hat{\mathbf{P}}(7,7)\hat{\mathbf{P}}(8,8) + \hat{\mathbf{P}}^2(1,2) + \hat{\mathbf{P}}^2(4,5) + \\
& \hat{\mathbf{P}}^2(7,8) + 2\hat{\mathbf{P}}(1,4)\hat{\mathbf{P}}(2,5) + 2\hat{\mathbf{P}}(1,7)\hat{\mathbf{P}}(2,8) + 2\hat{\mathbf{P}}(1,5)\hat{\mathbf{P}}(2,4) + \\
& 2\hat{\mathbf{P}}(1,8)\hat{\mathbf{P}}(2,7) + 2\hat{\mathbf{P}}(5,8)\hat{\mathbf{P}}(4,7) + 2\hat{\mathbf{P}}(5,7)\hat{\mathbf{P}}(4,8) \qquad (8)
\end{aligned}$$

Matrix $\mathbf{H}$ in this case is:

$$\mathbf{H}(\hat{\mathbf{s}}) = \begin{bmatrix} 1 & 0 & 0 & 0 & 0 & 0 & 0 & 0 & 0 \\ 0 & 0 & 0 & 1 & 0 & 0 & 0 & 0 & 0 \\ 0 & 0 & 0 & 0 & 0 & 0 & 1 & 0 & 0 \\ \hat{\mathbf{s}}(2) & \hat{\mathbf{s}}(1) & 0 & \hat{\mathbf{s}}(5) & \hat{\mathbf{s}}(4) & 0 & \hat{\mathbf{s}}(8) & \hat{\mathbf{s}}(7) & 0 \end{bmatrix}$$

Cartesian filters both with and without the range-rate measurement (referred to as *CartesianRR* and *Cartesian* respectively) will be considered in this report.

3 IMM Logic for Manoeuvre Tracking

3.1 IMM Theory

The IMM approach to filtering has been shown to provide superior results over single model KFs when manoeuvring targets are being tracked. However there is some computational expense incurred, which may prevent the use of an IMM in certain applications. The goal here was just to examine further which coordinate system produced the best track quality for manoeuvring target tracking, and IMM was therefore a natural choice to use.

There are five main sections to a generic IMM algorithm, regardless of which coordinate system is utilised. They are [1, p. 461]:

(I) Calculation of mixing probabilities. Assume there are r interacting models in place. Here the probability that model i was in effect at the previous time step k, given that model j is in effect at the current time step $k+1$ (conditioned on all measurements up to k) is calculated:

$$\mu_{i|j}(k|k) = \frac{1}{\bar{c}_j} p_{ij}\mu_i(k) \qquad i,j = 1,\ldots,r \tag{9}$$

where each $\bar{c}_j$ is a normalising constant, each μ_i is a model probability and each p_{ij} is a model transition probability.

(II) Mixing.

Using state estimates ($\hat{x}^i(k|k)$) from the previous time step, the mixed states and covariances that are matched to each mode (i.e. one of the two filter models in this case) are calculated:

$$\hat{x}^{0j}(k|k) = \sum_{i=1}^{r} \hat{x}^i(k|k)\mu_{i|j}(k|k) \qquad j = 1,\ldots,r \tag{10}$$

$$P^{0j}(k|k) = \sum_{i=1}^{r} \mu_{i|j}(k|k)\left\{P^i(k|k) + [\hat{x}^i(k|k) - \hat{x}^{0j}(k|k)]\cdot[\hat{x}^i(k|k) - \hat{x}^{0j}(k|k)]'\right\} \tag{11}$$

where $j = 1,\ldots,r$.

(III) Mode-matched filtering.

The above estimates and covariances are then used as inputs to the two models and have $\hat{x}^j(k+1|k+1)$, $(j = 1,\ldots,r)$ as the outputs.The likelihood functions corresponding to the two filters are then calculated as:

$$\Lambda_j(k+1) = \mathcal{N}\left\{z(k+1); \hat{z}^j[k+1|k; \hat{x}^{0j}(k|k)], S^j[k+1; P^{0j}(k|k)]\right\} \tag{12}$$

where $\mathcal{N}\{\cdot\}$ stands for the Gaussian pdf, with mean $\hat{z}^j$ and covariance S^j.

(IV) Mode probability update.

The probability of each mode being the correct one is updated:

$$\mu_j(k+1) = \frac{1}{c}\Lambda_j(k+1)\bar{c}_j \qquad j = 1, \ldots, r \tag{13}$$

where c is the normalisation constant.

(V) State estimate and covariance combination.

The two estimates and covariances are finally combined, and these values are used as the actual output of the system. They are not actually part of the IMM algorithm recursions.

$$\hat{x}(k+1|k+1) = \sum_{j=1}^{r} \hat{x}^j(k+1|k+1)\mu_j(k+1) \tag{14}$$

$$\begin{aligned} P(k+1|k+1) = \sum_{j=1}^{r} \mu_j(k+1)\{&P^j(k+1|k+1) \\ &+ [\hat{x}^j(k+1|k+1) - \hat{x}(k+1|k+1)] \\ &\cdot [\hat{x}^j(k+1|k+1) - \hat{x}(k+1|k+1)]'\} \end{aligned} \tag{15}$$

A schematic description of the IMM algorithm is shown in Fig.1. Three types of IMM systems have been developed for the investigation. Each system is based on one quiescent and one manoeuvring model.

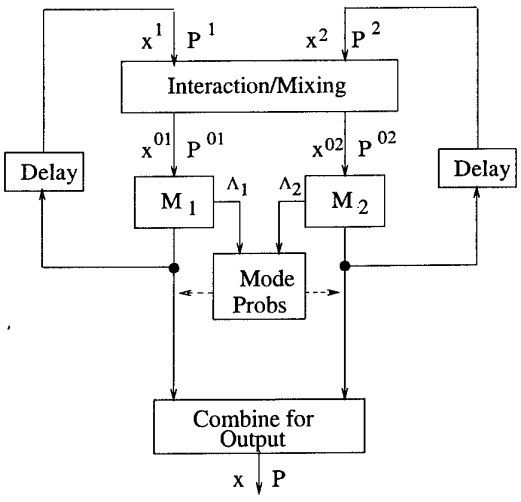

Figure 1: The IMM algorithm (with two models)

3.2 Implementation

Two different IMMs were implemented in Cartesian coordinates - one with two constant velocity models (*Imm2CV*) and the other with a constant velocity and a constant acceleration model (*ImmCVCA*). For the *Imm2CV* tracker, the approach was simple, as each model contained a nearly identical KF; mixing/interacting the state vectors and covariance matrices was straightforward. We used the constant velocity model (described in Sect. 2.2) with range-rate incorporation. The quiescent model (M1) has a quite small process noise standard deviation (for modelling constant velocity motion) while the manoeuvring model (M2) uses a fairly large amount of process noise for accommodating acceleration and higher order derivatives of velocity.

The quiescent model of *ImmCVCA* is identical to the quiescent model of *Imm2CV*. The constant acceleration model, with incorporated range-rate is described in Sect. 2.2. For steps (II) and (V) of the IMM algorithm above, the following approach was adopted. A truncated version of the constant acceleration model state vector and covariance matrix was created, with acceleration elements removed. Similarly, an expanded version of the constant velocity model's state vector and covariance matrix was formed, by adding zeros in place of the acceleration terms. This was so that state vectors (and associated covariances) were always of the same length and type during the mixing and interactions that occurred in these steps.

The approach used for the spherical tracker (*ImmSpher*) was slightly different. We again chose a dual model as in *Imm2CV* (quiescent model with low process noise and manoeuvring model with high process noise). However, due to the fact that we had 4 KF's operating in parallel (for each model of a spherical filter), it was necessary to adopt a different implementation of steps 2 and 5 of the IMM algorithm. It was decided to combine all four state vectors (and their associated covariance matrices) into one large vector (and one associated covariance matrix):

$$\mathbf{s}_{IMM} = [\mathbf{s}_R \;\; \mathbf{s}_{\lambda_N} \;\; \mathbf{s}_{\lambda_E} \;\; \mathbf{s}_{\lambda_D}]' \tag{16}$$

$$\mathbf{P}_{IMM} = \begin{bmatrix} \mathbf{P}_R & \mathbf{0} & \mathbf{0} & \mathbf{0} \\ \mathbf{0} & \mathbf{P}_{\lambda_N} & \mathbf{0} & \mathbf{0} \\ \mathbf{0} & \mathbf{0} & \mathbf{P}_{\lambda_E} & \mathbf{0} \\ \mathbf{0} & \mathbf{0} & \mathbf{0} & \mathbf{P}_{\lambda_D} \end{bmatrix} \tag{17}$$

This vector and its associated covariance was kept together for all IMM mixing and interaction, but was split into component vectors for actual KF routines, as per normal.

In both spherical and Cartesian IMM systems, the Markov chain transition matrix (used to obtain the p_{ij} in eqn. 9) was:

$$\mathbf{p} = \begin{bmatrix} 0.95 & 0.05 \\ 0.05 & 0.95 \end{bmatrix} \tag{18}$$

For initialisation of all IMM filters, a probability of 0.1 was assigned to the quiescent model (M1) and a probability of 0.9 to the manoeuvring model (M2).

The following filter parameters were used for all trackers (both single trackers and IMM systems): $\tau_R = 5$ (sec), $\tau_m = 5$ (sec). State vector initialisation for spherical filters was performed using two point differencing [1, Sec. 5.5.3] in the range/range-rate filter and three point differencing for the direction cosines. For Cartesian, two point and three point differencing was used for constant velocity and constant acceleration models respectively.

When two point differencing was used, the initial value for the state vector covariance matrix, $\mathbf{P}_0$, was determined according to [1, eqn. (5.5.3-5)]. The appropriate formula for the case of three point differencing was found to be:

$$\mathbf{P}_0 = \begin{bmatrix} r & r/T & r/T^2 \\ r/T & 2r/T^2 & 3r/T^3 \\ r/T^2 & 3r/T^3 & 6r/T^4 \end{bmatrix} \tag{19}$$

where r is the variance of the measurement noise. Note that eqn. 19 corresponds to the initial direction cosine state vectors in the spherical filters, or as part of the x, y, z state vector in Cartesian filters.

3.3 Gating

Data validation (or *gating*) was incorporated into the filters. Gating was performed on the (combined) x, y and z components of the state vector in the Cartesian filters and for range and the three direction cosines in spherical filters. Ellipsoidal gating with a probability of gating of $P_G = 0.995$ was used in each case. Track loss was declared when three non-gated measurement events occurred consecutively. The process noise used in gating for *ImmSpher* and *Imm2CV* was the same value used for tracking with the manoeuvring model. Gating for *ImmCVCA* was performed using a constant velocity model only and the process noise was the same as that used for gating in *Imm2CV*. All single trackers (i.e. those described in Section 2) use the relevant values from their normal tracking algorithm for gating.

Finally, it should be noted that the trackers continued tracking when track loss was reported. The reason for this was that the interest lay not in simulating totally realistic operational trackers, but in comparing track accuracy between coordinate systems. Thus the data obtained from those Monte Carlo runs where track loss occurred was still included in the ensemble of results used for error calculations.

4 Computer Simulations

The simulations employed MATLAB routines to generate APDR sensor like data and to process (and display) that data according to the aforementioned systems.

4.1 Method of Comparison

The criteria for comparing tracking in the two coordinate systems were the following track errors: positional, horizontal heading, vertical heading and range-rate. Monte Carlo simulations were performed with a new set of APDR measurements for each run. For every trial, 1000 runs were generated as input to the relevant tracking systems. The ensemble of results was averaged at each time point. Positional error represents the average Euclidean distance between the true and estimated target location. Heading and range-rate errors on average are zero and so their root mean square (RMS) values were calculated. The plots presented in this report display a comparison of those errors versus time.

For the case of a manoeuvring target trajectory (i.e. the IMM systems comparison), the switching of model probabilities (i.e. μ_1 and μ_2 defined by eqn. 13) were also examined.

In terms of the simulated radar sensor data, the measurement noise standard deviations used were based on typical values found in an APDR operating in either HPRF or MPRF mode [11, Chps. 27,28]. The measurements were multivariate Gaussian, mutually independent with mean of (ρ_m, $\dot{\rho_m}$, θ_m, ϵ_m) equal to the corresponding trajectory kinematic state. The standard deviations adopted for HPRF were: $\sigma_\rho = 1.5$ km, $\sigma_{\dot{\rho}} = 3.6$ km/h, $\sigma_\theta = 2°$, $\sigma_\epsilon = 2°$. For MPRF the values used were: $\sigma_\rho = 0.06$ km, $\sigma_{\dot{\rho}} = 18$ km/h, $\sigma_\theta = 2°$, $\sigma_\epsilon = 2°$. Note that the HPRF (versus MPRF) was characterised by larger range error and smaller range-rate error. The update interval of the measurements was set to 3 seconds. For simplicity, a unity probability of detection and a static observer case was assumed.

To give an indication of the overall benefits of using IMM for manoeuvre tracking, the IMM results were compared with those obtained using a single model tracker of the same type used in the IMM. In other words, the performance obtained from a single process noise model was compared with the two interacting models, for both Cartesian and spherical coordinate systems.

4.2 Simulated Trajectories

Three different trajectories were chosen for this investigation. The first was a constant velocity trajectory, with the target moving towards the stationary radar platform (see Figure 2). The starting range was approximately 82 km and the final range about 6 km from the radar platform. The target's speed was approximately 640 km/h in the North/East plane, with zero Down velocity, at a (constant) height of 3 km above the radar. Simulations using this trajectory were run with both MPRF and HPRF modes assumed operating.

The second trajectory consisted of two simple manoeuvres. The target, shown in Figure 3 began at a range of approximately 81 km and headed with constant velocity of about 1300 km/h towards the radar platform, until it reached a range of approximately 20 km. It then performed a 90° $2g$ turn followed by a short constant velocity heading, then another 90° turn, but at $5g$, so that it is headed away from the platform. It then continued on a constant velocity heading until it was roughly 81 km away from the radar again. The main purpose of this trajectory was to show the response of the filters to a target changing from non-manoeuvring to manoeuvring motion, and vice versa.

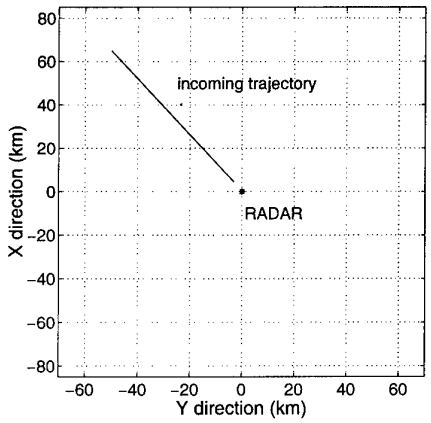

Figure 2: Top-down view of Trajectory 1

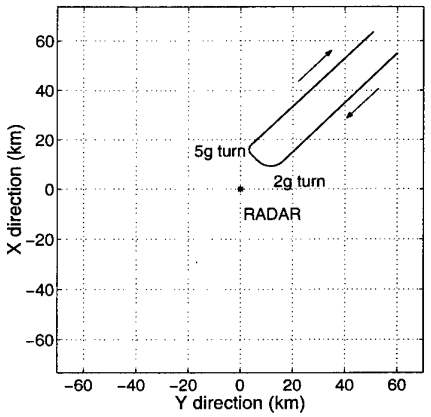

Figure 3: Top-down view of Trajectory 2

Since the target moves away from the APDR platform during the second trajectory, it was decided to simulate only MPRF mode measurements, as HPRF mode would be "blind" in the tail chase and therefore not be used in such a scenario.

The third scenario is taken directly from the benchmark trajectories explored in [4]. The trajectory referred to as number 6 in [4] was chosen and Figure 4 shows the top down view. A summary of this trajectory is as follows: constant velocity, $7g$ turn, constant velocity, $6g$ turn and reduced speed/vertical dive then level flight again, $6g$ turn and full throttle/constant heading, $7g$ turn, constant velocity. Again only the MPRF mode was considered for this scenario.

4.3 Simulation Results

A brief discussion and summary of the comparison of errors is now presented. Unless otherwise stated, the comments refer to that portion of time after which it was deemed obvious that the filters had "settled".

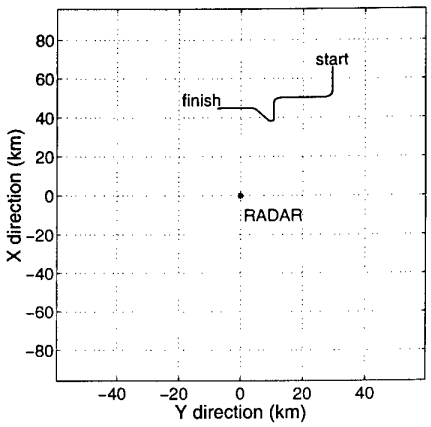

Figure 4: Top-down view of Trajectory 3

4.3.1 Non-manoeuvring Target Trajectory

The results for Trajectory 1 can be seen in Figures 5 and 6, and show errors for HPRF and MPRF mode trials respectively. The process noise standard deviation used for all three filters was $\sigma_m = 0.4g$.

Trial 1(a) (HPRF, Figure 5)

For positional error, it is noted that *CartesianRR* is better than *Cartesian* and *Spherical*, although the latter improves at very close range. *Cartesian* also gets worse at around the same point in tracking. Both Cartesian trackers give virtually identical horizontal / vertical heading errors. They clearly perform much better than *Spherical*, whose error is up to about 5° worse. For range-rate error, we see that *CartesianRR* converges to a steady-state value (generally equal to that of *Spherical*) fairly quickly. The performance of *Cartesian* is quite poor—when it does reach a steady-state the level is an order of magnitude higher than the other trackers. *Spherical* performs the best here, because its error is constant (and very small). This result is understandable since *Spherical* directly tracks the range and range-rate.

There was no track loss reported for any tracker in this trial.

Trial 1(b) (MPRF, Figure 6)

The positional errors of the two Cartesian trackers are virtually identical and are slightly better than *Spherical*. The performances in horizontal/vertical heading errors are generally identical to the HPRF case (Trial 1(a)), that is, Cartesian trackers are much more accurate than spherical. Results for range-rate error are markedly different however. *CartesianRR* settles to a value slightly lower than *Spherical*, which is again fairly constant. However, both are at levels around 10 km/h higher than for HPRF. The performance of *Cartesian* is similar to *CartesianRR* but the error for *Cartesian* grows larger as range decreases. Again, these results are expected because MPRF mode has much higher range-rate errors than HPRF mode.

There was either zero or negligible track loss reported for the trackers in this trial.

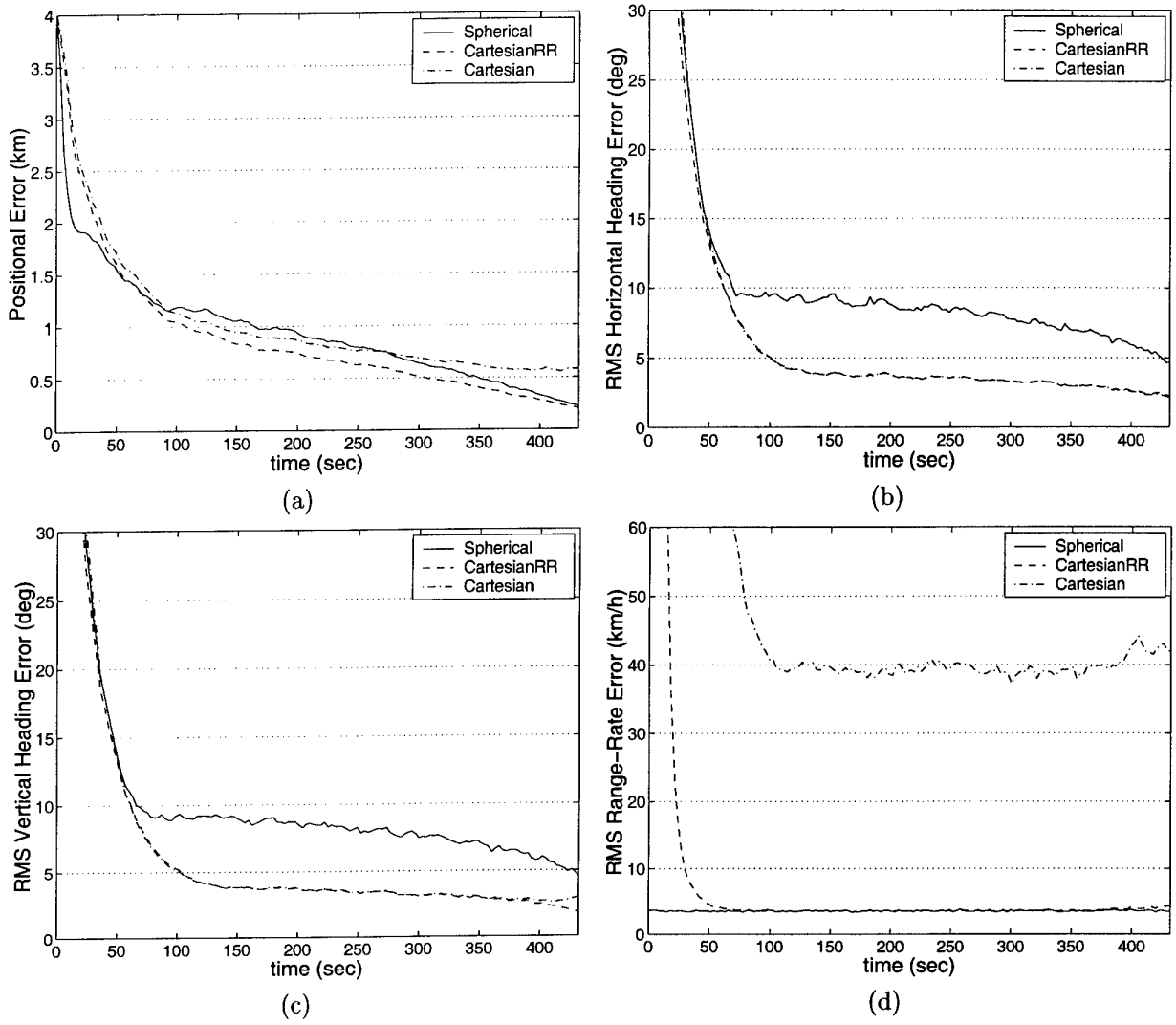

Figure 5: Trial 1(a) (HPRF) tracking errors: (a) positional; (b) horizontal heading; (c) vertical heading; (d) range-rate

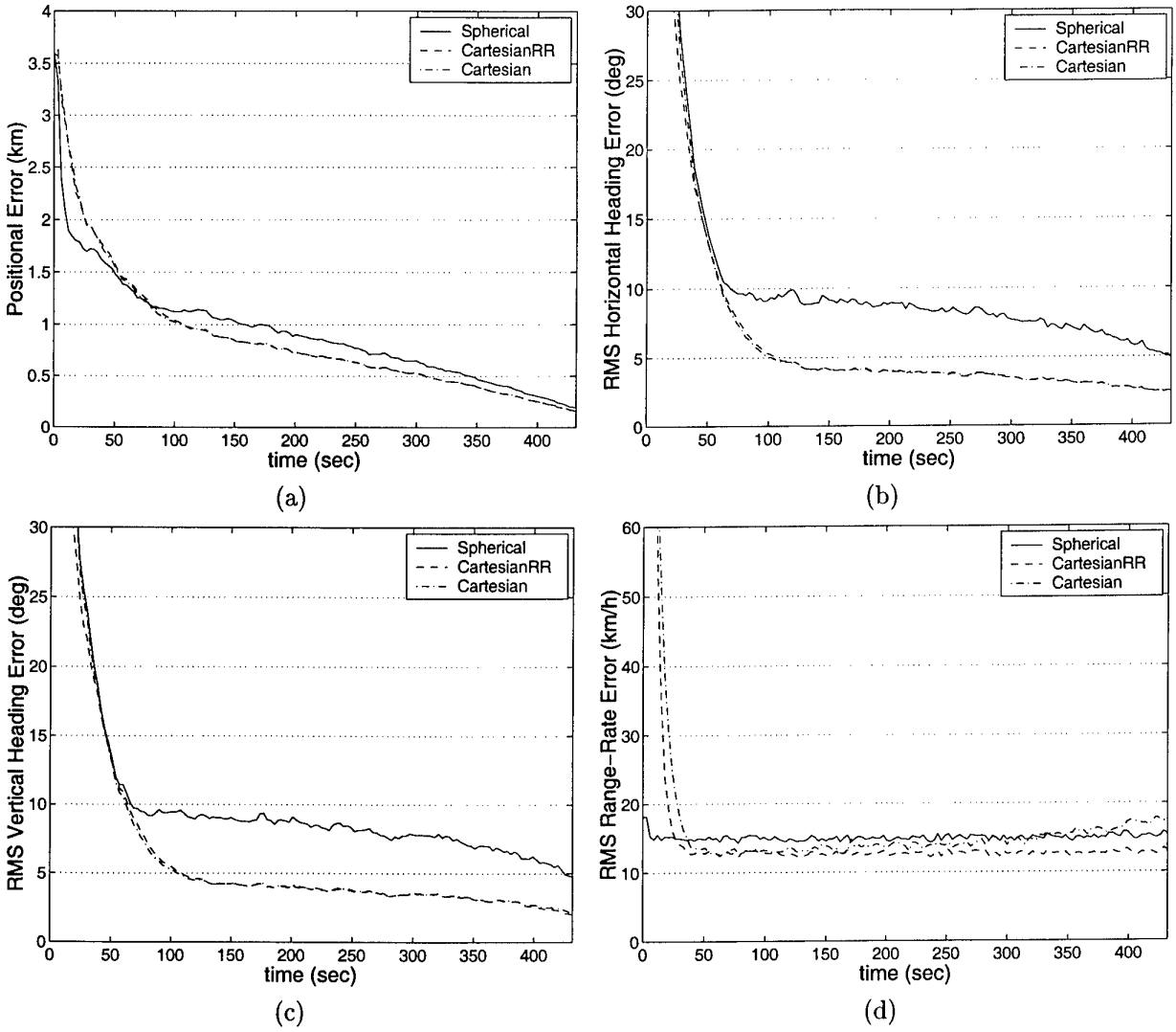

Figure 6: Trial 1(b) (MPRF) tracking errors: (a) positional; (b) horizontal heading; (c) vertical heading; (d) range-rate

4.3.2 Manoeuvring Target Trajectories

For the last two trajectories, the three IMM trackers were compared, as well as *CartesianRR* and *Spherical*. The process noise levels (i.e. σ_m) chosen for the various trackers were as follows:

Table 1: Process Noise Levels

TRACKER	Process Noise M1	Process Noise M2
ImmSpher	$0.1g$	$2.5g$
Imm2CV	$0.1g$	$2.5g$
ImmCVCA	$0.1g$	$1.5g$
CartesianRR	$1.5g$	
Spherical	$1.5g$	

Trial 2 (MPRF) - Trajectory 2

The model probabilities versus time, for each of the three IMM trackers can be seen in Figure 7. The initial switching at the start of each plot is due to the fact that the initial model probabilities were deliberately set to 0.1 and 0.9 for M1 and M2 respectively. The reasons for this were twofold. Firstly, it is safer to assume that the target may actually be manoeuvring when the tracking begins. Secondly, by using this assumption, a larger filter bandwidth (due to the higher process noise standard deviation of M2) is essentially used to begin with, which usually helps to reduce settling errors of the filters.

The bottom plot in Figure 7 shows the magnitude of acceleration versus time, for the trajectory under consideration. The vertical lines indicate approximate start and stop times of manoeuvres (i.e. non-zero accelerations). The values given are an approximation only, since actual acceleration was not generated in the state vector for this trajectory. In terms of the switching performance, it is clear that both Cartesian trackers switch very sharply and reliably detect the first manoeuvre (i.e. the $2g$ turn). However, it would seem that due to the time it takes to switch back to M1, the trackers do not accurately detect that the target has stopped turning before the next manoeuvre begins.

The error versus time plots for Trial 2 are displayed as follows: Figure 8 shows a comparison of the three IMM trackers, Figure 9 shows a comparison of *Imm2CV* with *CartesianRR* and Figure 10 shows a comparison of *ImmSpher* with *Spherical*.

As a general comment (for both Trial 2 and Trial 3), although manoeuvring and non-manoeuvring sections of the tracking errors are referred to, they do not always correspond to the relevant sections of the target trajectory. The reason for this is that the IMM filters generally have a lag in switching to the manoeuvring model (M2) and also a large settling time in returning to M1.

In comparing the three IMM trackers, the following is noted. All three trackers have very similar positional errors during the non-manoeuvring periods, with *ImmCVCA* doing slightly better than the other two. During the manoeuvring periods, *ImmSpher* performs best, followed by *ImmCVCA*, then *Imm2CV*. The last tracker's performance on the second turn is particularly bad. A similar general trend is seen for horizontal heading error. During non-manoeuvring periods, vertical heading errors for *ImmCVCA* and *Imm2CV*

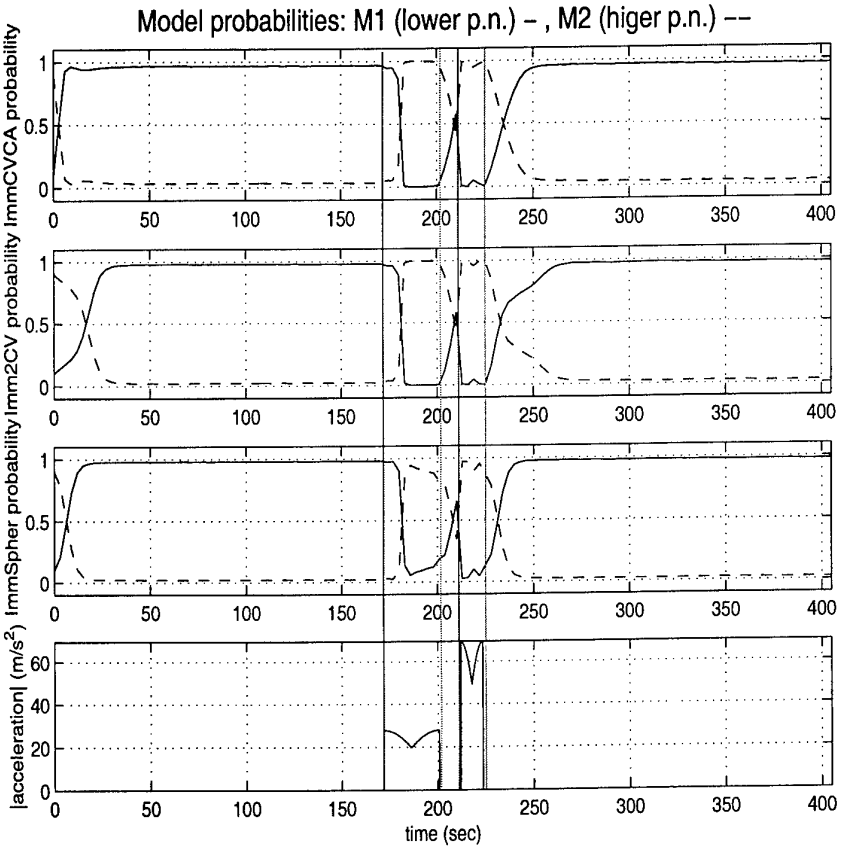

Figure 7: Trial 2 model probabilities

are virtually identical, and are generally a little better than *ImmSpher*. Overall *Imm2CV* performs best during the manoeuvring sections followed by *ImmCVCA*, then *ImmSpher*. For range-rate error, *ImmCVCA* and *Imm2CV* are very similar during non-manoeuvring periods and clearly do better than *ImmSpher*. However, the latter performs best during the manoeuvring sections, with *ImmCVCA* doing worst.

By examining the trends in the plots of Figure 9, it can be seen that in general, *Imm2CV* has better error performance during non-manoeuvring periods. There is not much useful gain to be had during the manoeuvres because the errors for *Imm2CV* are still very high, despite being (usually) lower than *CartesianRR*. It must stressed however, that *CartesianRR* actually lost track almost half of the time for Trial 2. So it could be argued that to track such a trajectory realistically, a single model tracker with moderate process noise ($1.5g$ here for *CartesianRR*) is inappropriate.

A similar situation presents itself in the plots of Figure 10, where *ImmSpher* and *Spherical* are compared, although both trackers had acceptable track loss in this case. Only for vertical heading error was *Spherical* (slightly) better than *ImmSpher*.

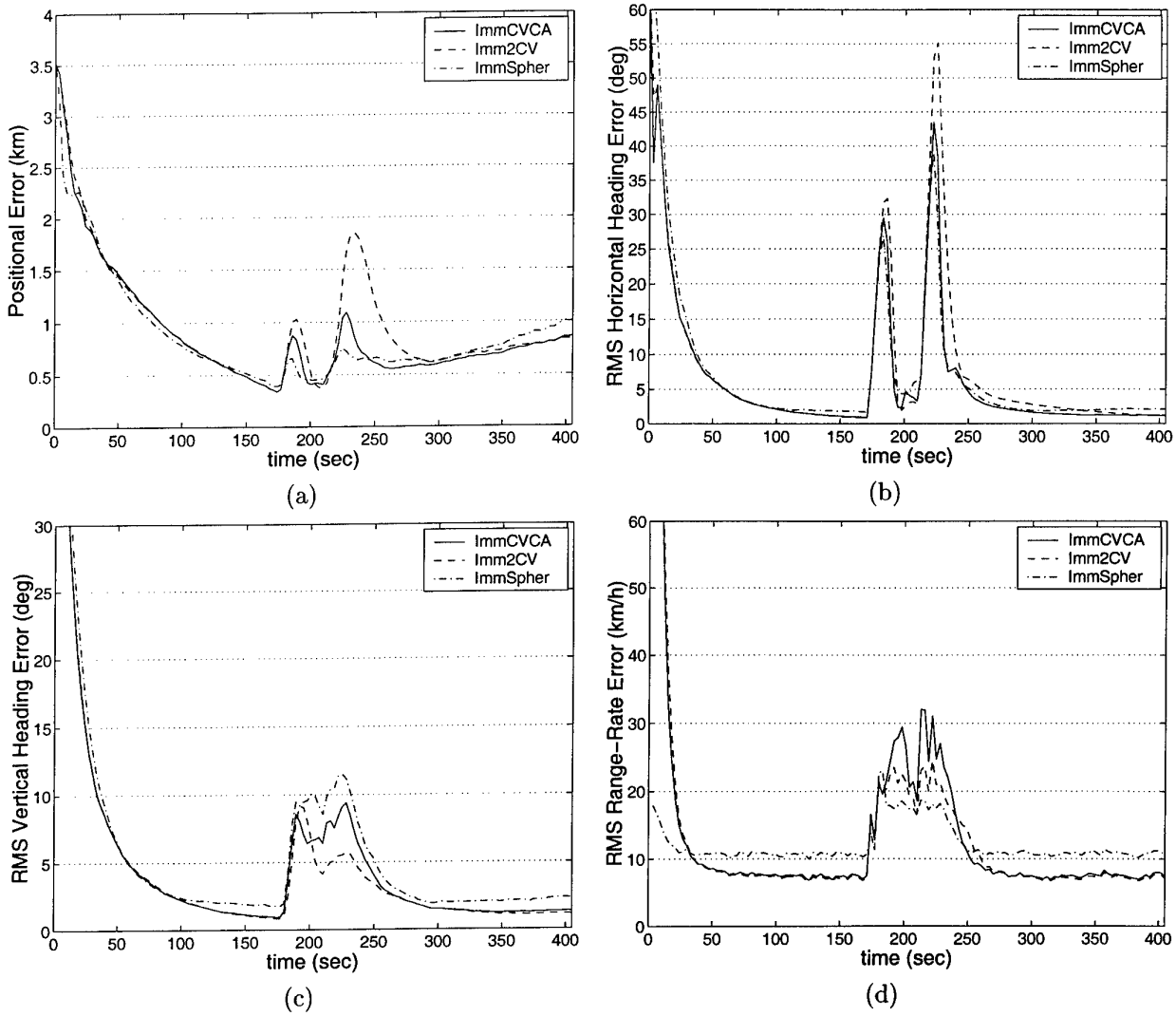

Figure 8: Trial 2 tracking errors (IMM filters): (a) positional; (b) horizontal heading; (c) vertical heading; (d) range-rate

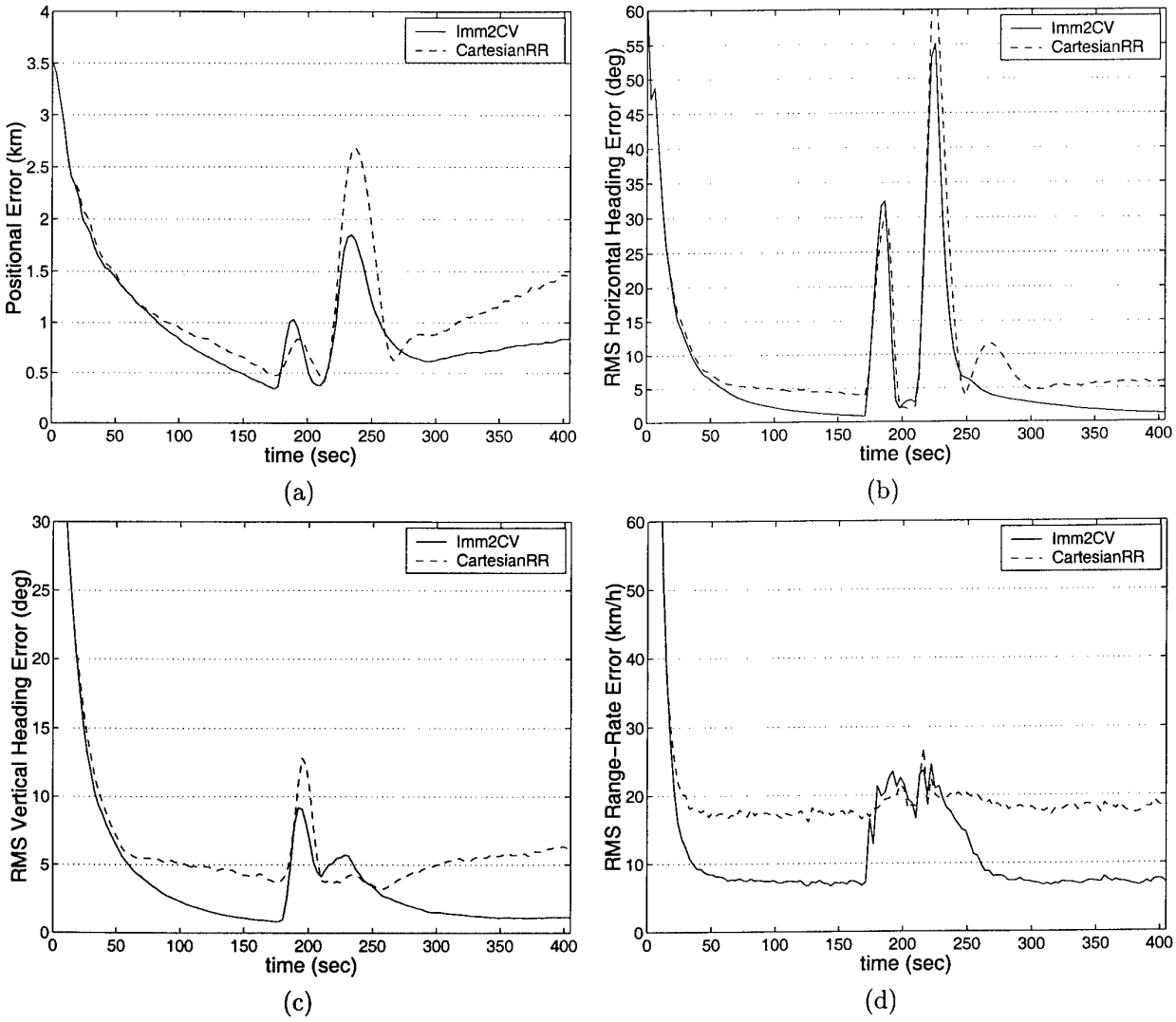

Figure 9: Trial 2 tracking errors (Cartesian filters): (a) positional; (b) horizontal heading; (c) vertical heading; (d) range-rate

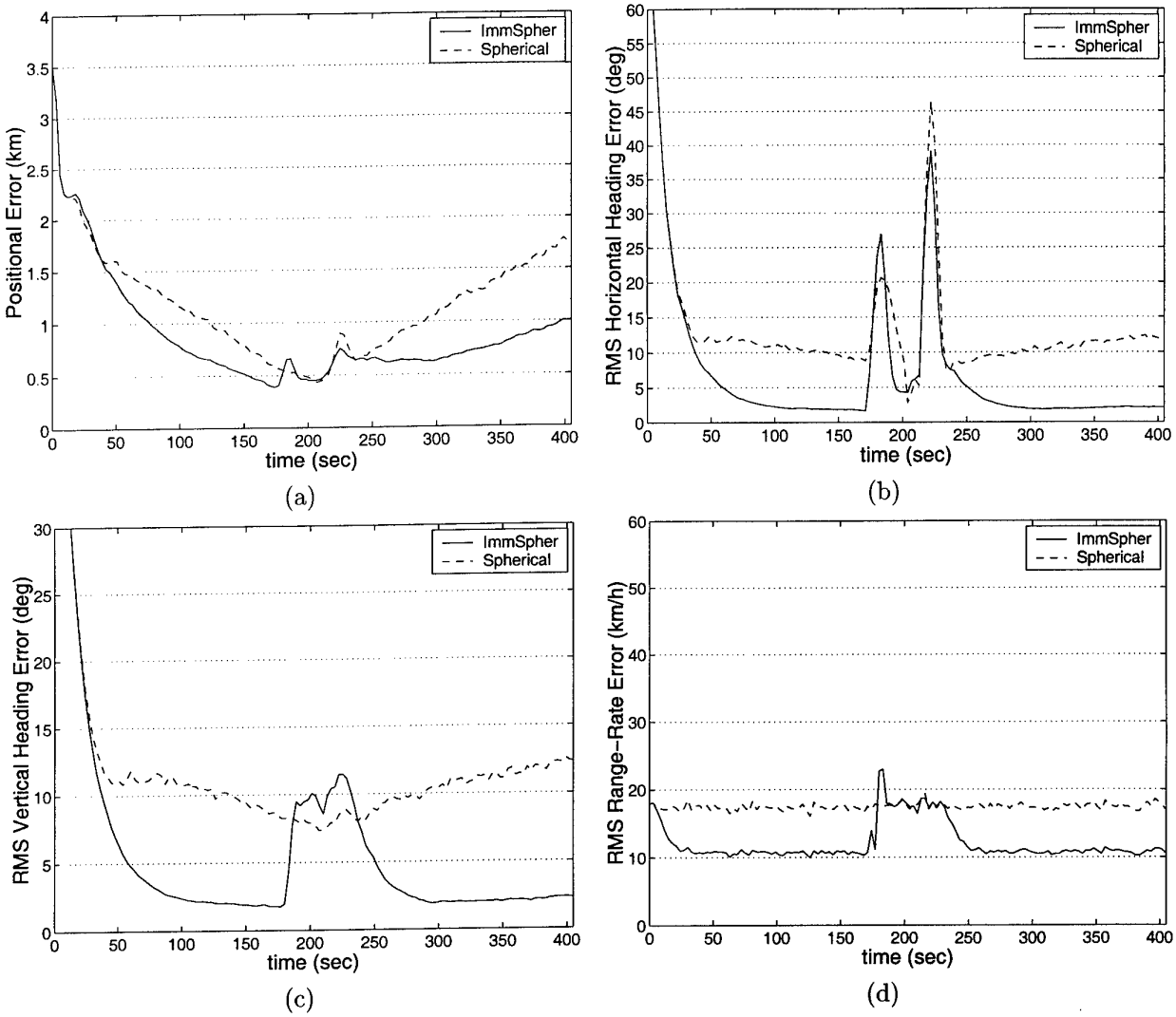

Figure 10: Trial 2 tracking errors (spherical filters): (a) positional; (b) horizontal heading; (c) vertical heading; (d) range-rate

Table 2: Track Loss Statistics for Trial 2

TRACKER	Track Loss
ImmSpher	0%
Imm2CV	2.9%
ImmCVCA	0%
CartesianRR	48.4%
Spherical	0%

Trial 3 (MPRF) - Trajectory 3

Figure 11 shows the model probabilities versus time. The initial probabilities were set to the same values as for Trial 2.

The bottom plot in Figure 11 shows the magnitude of acceleration versus time, for the trajectory under consideration. The values given are taken directly from the generated data for the benchmark trajectory. The plots show that switching was in general not as sharp and clean as that seen for Trial 2. This was probably due to the fact that there were a larger number of fairly closely spaced accelerations (manoeuvres) present in this trajectory, and therefore the trackers could not 'decide' easily which state the target was in. The best switching performance is arguably obtained by *ImmCVCA* since it detects the four main manoeuvres very well and switches back to M1 the quickest after the last manoeuvre.

The error versus time plots for Trial 3 are displayed as follows: Figure 12 shows a comparison of the three IMM trackers, Figure 13 shows a comparison of *Imm2CV* with *CartesianRR* and Figure 14 shows a comparison of *ImmSpher* with *Spherical*.

The comparison of the IMM trackers in Figure 12 highlights some interesting results. Positional errors are generally quite high compared to those found in Trial 2. *ImmSpher* performs better on the first two manoeuvres. The two Cartesian trackers are characterised by very large errors after a manoeuvre is performed. Horizontal heading errors are very large for all trackers during manoeuvring periods. *ImmSpher* again performs best on the first two manoeuvres but is the worst on the last manoeuvre. For vertical heading, errors are quite large, and there is no clear winner in terms of performance of *Imm2CV* versus *ImmSpher*. Finally, for range-rate error, *ImmSpher* does best, followed by *Imm2CV* and *ImmCVCA*.

Overall there are no long "quiet" periods in terms of the trackers settling to small error values. This is because there are too many manoeuvres too often for the filters to settle (this correlates with the observed switching of models, discussed earlier).

The main conclusion to draw from the plots of Figures 13 and 14 is that it appears there is not much benefit in using IMM over the single Cartesian or spherical tracker in this scenario, since for this trajectory the non-manoeuvring sections are not long enough to bring out the benefit of the low process noise in M1.

Examining the data in Table 3, we see that *Imm2CV* and *CartesianRR* are the only trackers where significant track loss occurs for Trial 3.

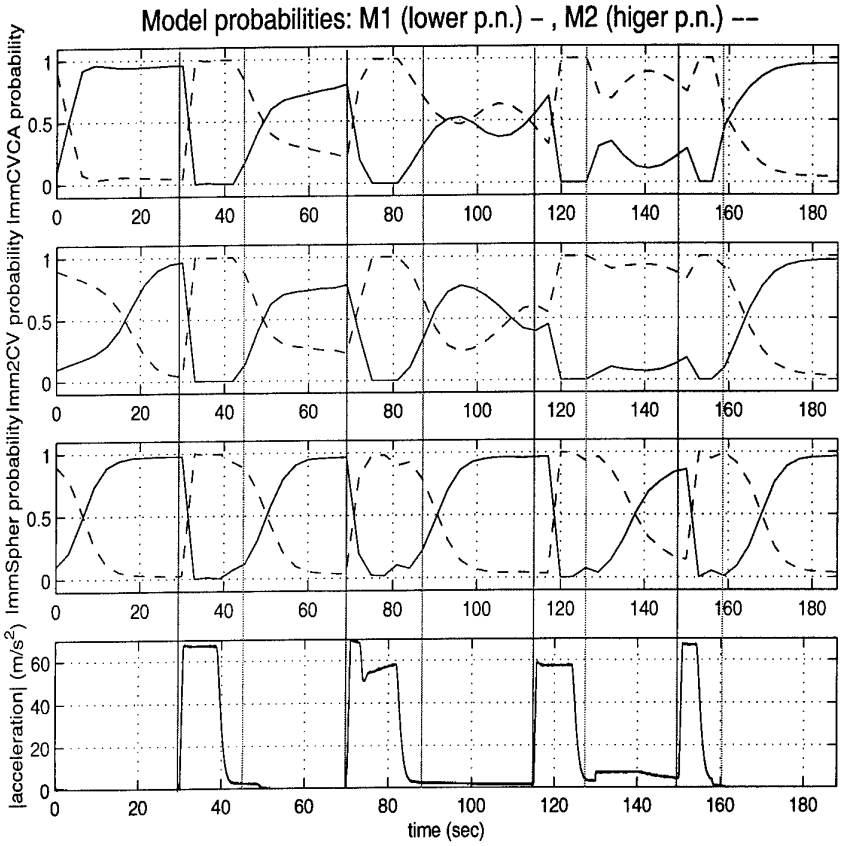

Figure 11: Trial 3 model probabilities

4.4 Computational Aspects

The data presented in Table 4 gives a very rough estimate of the relative amount of computation needed for each tracking system, with *Spherical* used as a reference due to its requiring the least amount of computation. Note that this is a guide only, and proper methodical comparisons were not undertaken. However, the general trends should be obvious.

It is also necessary to mention that the tracking was performed in units of kilometres (as well as seconds and radians). Distances for the trajectory data were generated or obtained (in the case of Trial 3) in metres. However, tracking in this unit amplified certain undesirable occurrences for positional error in spherical coordinates. Investigations suggest that although the phenomenon is influenced by other factors, the choice of distance units has an unexpected and unexplainable effect. It is believed therefore that the effect may be attributable to numerical instability within MATLAB.

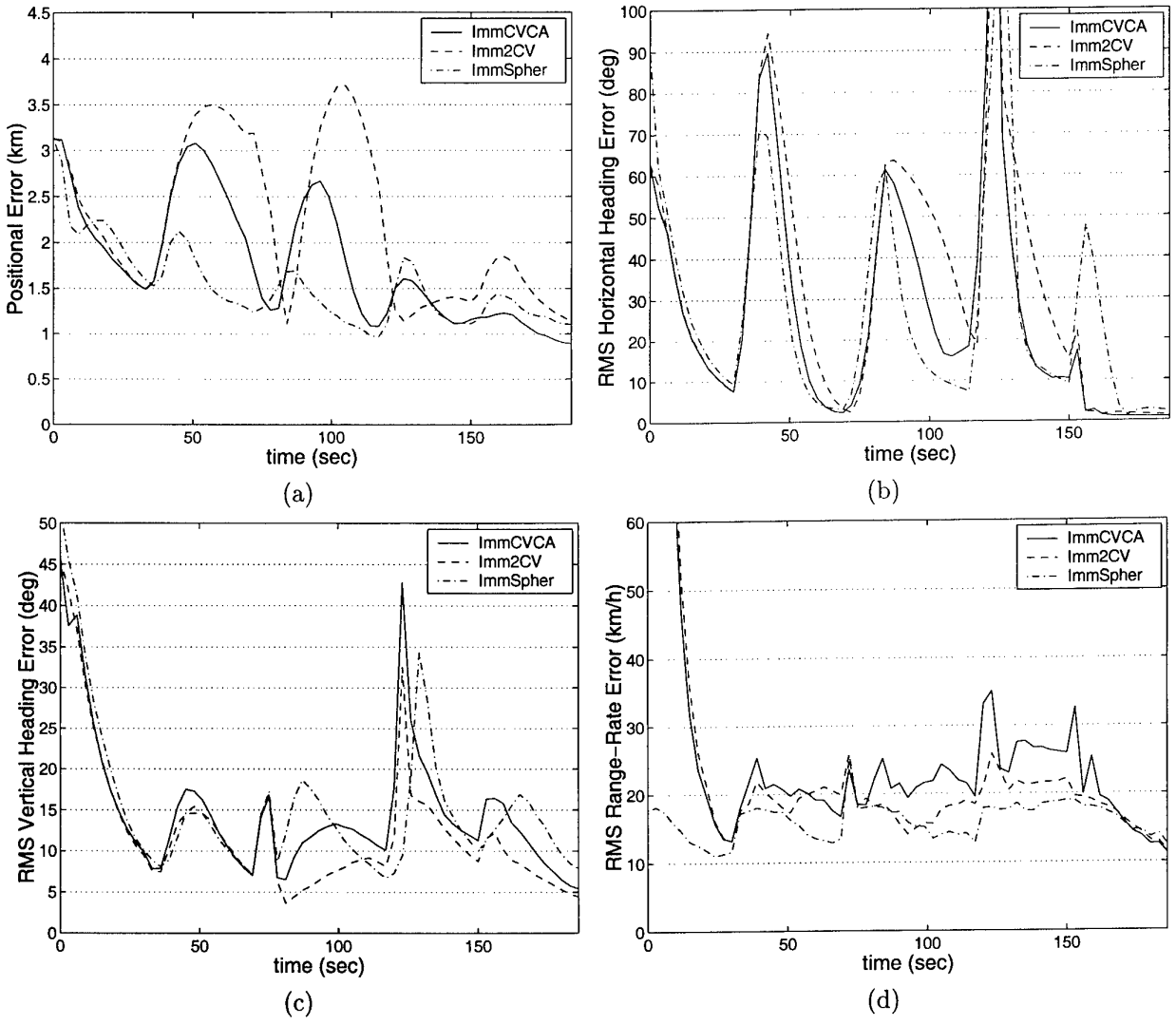

Figure 12: Trial 3 tracking errors (IMM filters): (a) positional; (b) horizontal heading; (c) vertical heading; (d) range-rate

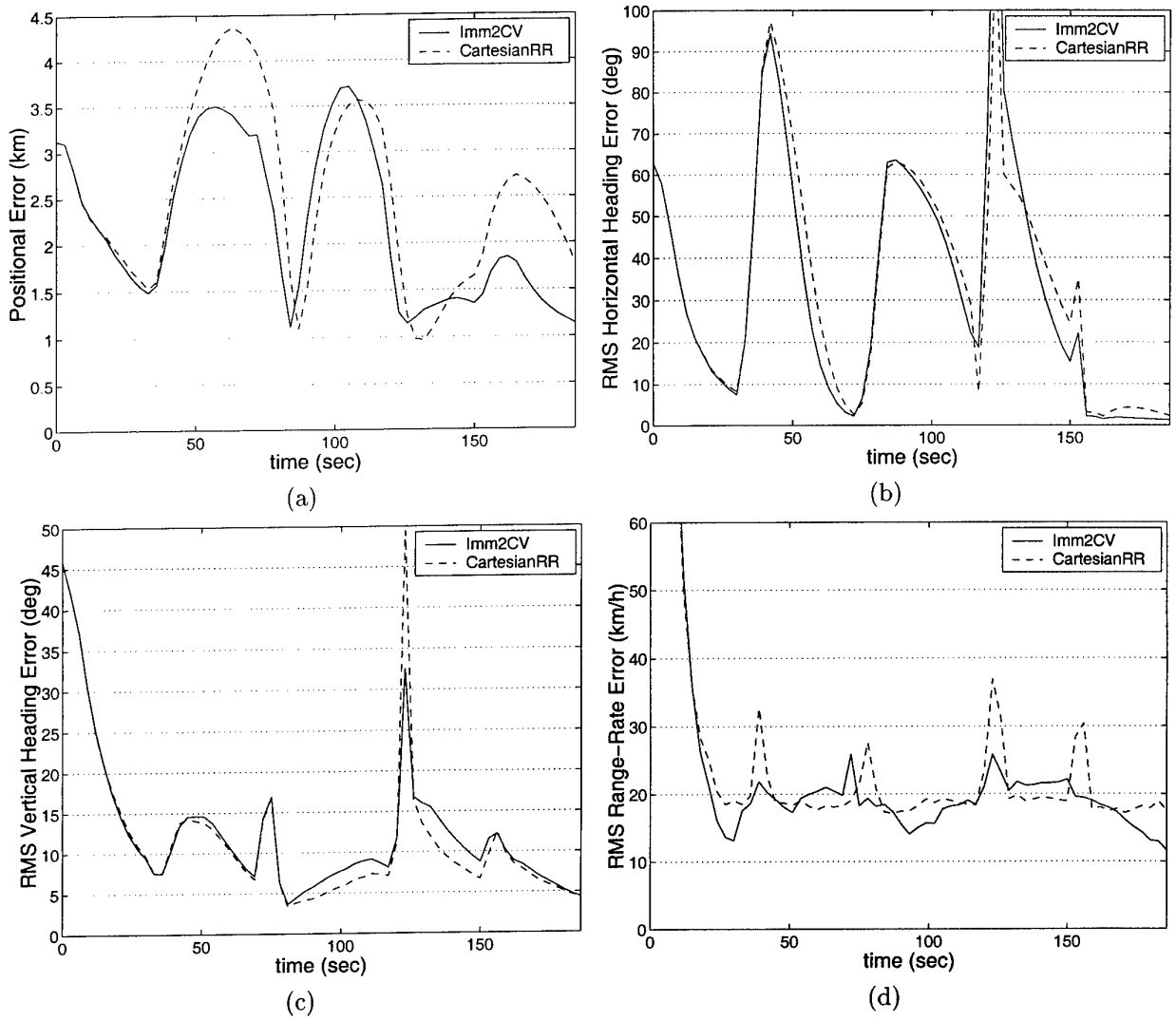

Figure 13: Trial 3 tracking errors (Cartesian filters): (a) positional; (b) horizontal heading; (c) vertical heading; (d) range-rate

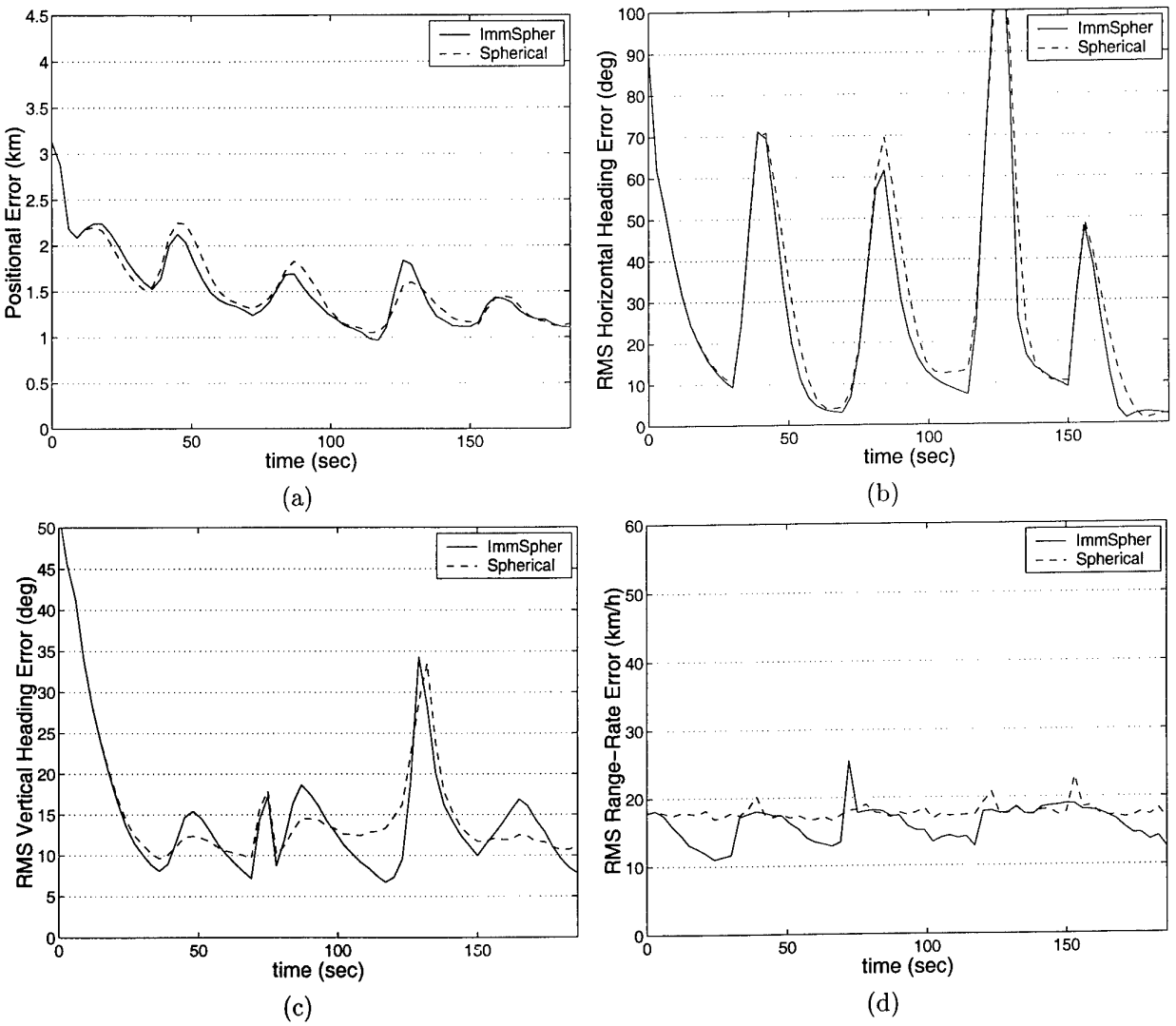

Figure 14: Trial 3 tracking errors (spherical filters): (a) positional; (b) horizontal heading; (c) vertical heading; (d) range-rate

Table 3: Track Loss Statistics for Trial 3

TRACKER	Track Loss
ImmSpher	0%
Imm2CV	7.3%
ImmCVCA	0.1%
CartesianRR	7.6%
Spherical	0%

Table 4: Relative Computational Requirements

TRACKER	Relative Computations Needed
Spherical	1
Cartesian	2
CartesianRR	3
ImmSpher	7
Imm2CV	8
ImmCVCA	11

5 Conclusions

For constant velocity target tracking, it appears that there is useful error reduction to be had by using Cartesian coordinates over spherical. It is noteworthy that the inclusion of range-rate into the Cartesian tracker is of significant benefit only for the HPRF mode.

The general trend for manoeuvring trajectory motion is that spherical coordinate filters achieve higher tracking accuracy during manoeuvres (or at least when the tracker is responding to them). During manoeuvres, the spherical filters also appear to be more robust against track loss. For tracking in Cartesian coordinates, tracks are occasionally lost if the manoeuvring model is too simplistic (such as the constant velocity model with large process noise). The constant acceleration model for a manoeuvring target in Cartesian coordinates, however, performs reasonably well during manoeuvres. Other dynamic models in the Cartesian IMM algorithm have not been investigated in the report, though the literature suggests that some improvements could be expected using constant jerk [10] or constant speed turning models [5] for tracking highly manoeuvrable targets.

Overall tracking in spherical coordinates with an airborne pulse Doppler radar seems to be a reasonable choice - even the most severe manoeuvres are tracked with no track loss and with the smallest tracking errors, while the computational load of the spherical filters is minimal. The main disadvantage of spherical coordinates is somewhat larger tracking errors for non-manoeuvring segments of a trajectory.

References

1. Y. Bar-Shalom and X. R. Li. *Estimation and Tracking.* Artech House, 1993.

2. S. Blackman and R. Popoli. *Design and Analysis of Modern Tracking Systems.* Artech House, 1999.

3. S. S. Blackman. *Multiple Target Tracking with Radar Applications.* Artech House, 1986.

4. D. Blair and G. A. Watson. Benchmark problem for radar resource allocation and tracking maneuvering targets in the presence of ecm. Technical Report NSWCDD/TR-96/10, Naval Surface Warfare Center Dahlgren Division, Systems Research and Technology Department, Sep. 1996.

5. W. D. Blair and G. A. Watson. IMM algorithm for solution to benchmark problem for tracking maneuvering targets. In *Proc. SPIE*, volume 2221, pages 476–488, 1994.

6. E. Brookner. *Tracking and Kalman filtering made easy.* John Wiley & Sons, 1998.

7. M. Brunet-Crespin. Multisensor tracking systems: coordinate system choice influence. In *Proc. Int. Conf. Radar, Soc. Electr. & Electron.*, pages 437–441, Paris, France, 1994.

8. A. Farina and F. A. Studer. *Radar Data Processing.* John Wiley, 1985.

9. D. Lerro and Y. Bar-Shalom. Tracking with debiased consistent converted measurements versus EKF. *IEEE Trans. Aerospace and Electronic Systems*, 29(3):1015–1022, July 1993.

10. K. Mehrotra and P. R. Mahapatra. A jerk model for tracking highly maneuvering targets. *IEEE Trans. Aerospace and Electronic Systems*, 33(4):1094–982, Oct. 1997.

11. G. W. Stimson. *Introduction to Airborne Radar.* Scitech Publishing, 2nd edition, 1998.

12. P. Suchomski. Explicit expressions for debiased statistics of 3D converted measurements. *IEEE Trans. Aerospace and Electronic Systems*, 1:368–370, Jan. 1999.

13. L. Mo X., Song, Y. Zhou, Z. K. Sun, and Y. Bar-Shalom. Unbiased converted measurements for tracking. *IEEE Trans. Aerospace and Electronic Systems*, 34(3):1023–1027, July 1998.

DISTRIBUTION LIST

On the Choice of the Coordinate System and Tracking Filter for the Track-while-scan Mode of an Airborne Pulse Doppler Radar

Steven Zollo and Branko Ristic

	Number of Copies
DEFENCE ORGANISATION	
Task Sponsor	
Gp Capt John Quaife, DACD	1
Gp Capt Clive Rossiter	1
S&T Program	
Chief Defence Scientist FAS Science Policy AS Science Corporate Management	1
Director General Science Policy Development	1
Counsellor, Defence Science, London	Doc Data Sht
Counsellor, Defence Science, Washington	Doc Data Sht
Scientific Adviser to MRDC, Thailand	Doc Data Sht
Scientific Adviser Policy and Command	1
Navy Scientific Adviser	Doc Data Sht
Scientific Adviser, Army	Doc Data Sht
Air Force Scientific Adviser	1
Director Trials	1
Aeronautical and Maritime Research Laboratory	
Director, Aeronautical and Maritime Research Laboratory	1
Chief, Weapons Systems Division	1
Dr Len Sciacca, HWSI	1
Ms Serena Stuart	1
Electronics and Surveillance Research Laboratory	
Director, Electronics and Surveillance Research Laboratory	Doc Data Sht
Chief, Surveillance Systems Division	1
Chief, Electronic Warfare Division	1
Research Leader, Wide Area Surveillance	1
Research Leader, Surveillance for Air Superiority	1
Dr John Percival, HTSF	1
Dr John Whitrow, HSSP	1
Author	4

Dr Martin Oxenham	1
DSTO Libraries	
Library Fishermans Bend	1
Library Maribyrnong	1
Library Salisbury	2
Australian Archives	1
Library, MOD, Pyrmont	Doc Data Sht
Capability Development Division	
Director General Aerospace Development	1
Director General Maritime Development	Doc Data Sht
Director General Land Development	Doc Data Sht
Director General C3I Development	Doc Data Sht
Navy	
Army	
ABCA Standardisation Officer, Puckapunyal	4
NAPOC QWG Engineer NBCD c/- DENGRS-A, HQ Engineer Centre Liverpool Military Area, NSW 2174	Doc Data Sht
Air Force	
Intelligence Program	
DGSTA	1
Manager, Information Centre, Defence Intelligence Organisation	1
Acquisition Program	
Corporate Support Program (libraries)	
Officer in Charge, TRS, Defence Regional Library, Canberra	1
Officer in Charge, Document Exchange Centre	1
Additional copies for DEC for exchange agreements	
US Defense Technical Information Center	2
UK Defence Research Information Centre	2
Canada Defence Scientific Information Service	1
NZ Defence Information Centre	1
National Library of Australia	1
UNIVERSITIES AND COLLEGES	
Australian Defence Force Academy Library	1
Head of Aerospace and Mechanical Engineering, ADFA	1

Deakin University Library, Serials Section (M List)	1
Senior Librarian, Hargrave Library, Monash University	Doc Data Sht
Librarian, Flinders University	1

OTHER ORGANISATIONS

NASA (Canberra)	1
Australian Government Publishing Service	1
The State Library of South Australia	1
Parliamentary Library of South Australia	1

ABSTRACTING AND INFORMATION ORGANISATIONS

Library, Chemical Abstracts Reference Service	1
Engineering Societies Library, US	1
Materials Information, Cambridge Science Abstracts, US	1
Documents Librarian, The Center for Research Libraries, US	1

INFORMATION EXCHANGE AGREEMENT PARTNERS

Acquisitions Unit, Science Reference and Information Service, UK	1
Library – Exchange Desk, National Institute of Standards and Technology, US	1
National Aerospace Library, Japan	1
National Aerospace Library, Netherlands	1

SPARES

DSTO Salisbury Research Library	5

Total number of copies:	64

DEFENCE SCIENCE AND TECHNOLOGY ORGANISATION DOCUMENT CONTROL DATA				1. CAVEAT/PRIVACY MARKING
2. TITLE On the Choice of the Coordinate System and Tracking Filter for the Track-while-scan Mode of an Airborne Pulse Doppler Radar			3. SECURITY CLASSIFICATION Document (U) Title (U) Abstract (U)	
4. AUTHOR(S) Steven Zollo and Branko Ristic			5. CORPORATE AUTHOR Electronics and Surveillance Research Laboratory PO Box 1500 Salisbury, South Australia, Australia 5108	
6a. DSTO NUMBER DSTO–TR–0926	6b. AR NUMBER AR-011-191		6c. TYPE OF REPORT Technical Report	7. DOCUMENT DATE December, 1999
8. FILE NUMBER B9505/17/240	9. TASK NUMBER AIR 99/204	10. SPONSOR DACD	11. No OF PAGES 27	12. No OF REFS 13
13. DOWNGRADING / DELIMITING INSTRUCTIONS Not Applicable			14. RELEASE AUTHORITY Chief, Surveillance Systems Division	
15. SECONDARY RELEASE STATEMENT OF THIS DOCUMENT *Approved For Public Release* OVERSEAS ENQUIRIES OUTSIDE STATED LIMITATIONS SHOULD BE REFERRED THROUGH DOCUMENT EXCHANGE, PO BOX 1500, SALISBURY, SOUTH AUSTRALIA 5108				
16. DELIBERATE ANNOUNCEMENT No Limitations				
17. CITATION IN OTHER DOCUMENTS No Limitations				
18. DEFTEST DESCRIPTORS Target tracking Kalman filtering Modelling			Tracking filters Airborne radar	

19. ABSTRACT

A comparison between tracking in *spherical coordinates* using coupled range and angle filters and tracking with debiased consistent converted measurements in 3D *Cartesian coordinates* is presented. The sensor is an airborne pulse Doppler radar (APDR) with typical measurements being range, range-rate, azimuth and elevation. The report investigates the tracking accuracy (position, range-rate and vertical/horizontal heading) achievable in the Medium and High PRF mode of an APDR, for both non-manoeuvring and manoeuvring targets. The manoeuvre handling logic is based on the interactive multiple model (IMM) approach.